Adaptive Predictive Deadbeat Current Control of Single-Phase Multi-tuned Shunt Hybrid Active Power Filters

Mohammad-Sadegh Karbasforooshan, and Mohammad Monfared, *Senior Member, IEEE*

***Abstract*-- This paper suggests an adaptive predictive deadbeat current control method for single-phase multi-tuned shunt hybrid active power filters (HAPFs) to improve the power quality of single-phase and three-phase four-wire utility grids. The HAPF structure eliminates the resonance between the passive power filter and the grid impedance. Furthermore, it can be integrated into passive filters to enhance their filtering performance. In this paper, a digital algorithm is proposed for managing the performance of each converter leg accurately. To do so, an exact model of the high-order system is developed, and the transfer function of the plant is calculated in continuous and discrete time domains. Then, a predictive deadbeat technique for HAPF current control is presented, which benefits from high accuracy, fast dynamics, and low sensitivity to system parameter mismatches. Extensive simulation and experimental tests are conducted and the results match well to confirm the success and appropriate performance of the overall system. Also, performance comparison with conventional solutions demonstrates the superiority of the suggested filtering technique.**

***Index Terms*-- Adaptive control; predictive deadbeat control; hybrid active power filter; multi-tuned filter.**

NOMENCLATURE

PPF	Passive power filter
APF	Active power filter
HAPF	Hybrid active power filter
PCC	Point of common coupling
RCG	Reference current generation
THD	Total harmonic distortion
ESR	Equivalent series resistance
SOGI	Second-order generalized integrator
RLS	Recursive least square
PWM	Pulse-width modulation
i_S	Grid current
i_L	Load current
i_H	HAPF injected current
i_P	PPF inductor current
i_F	APF injected current
v_S	Grid voltage
v_{conv}	Converter output voltage
v_{dc}	Converter DC-link voltage

I. INTRODUCTION

NOWADAYS, different harmonic compensation solutions based on PPFs, APFs and HAPFs are proposed both by industry and academia. The PPFs, also known as single/multi-tuned LC filters, benefit from simplicity, high reliability and low cost. Although, their major drawbacks are parallel resonance with grid impedance, poor performance under light loads and/or small grid impedances and high sensitivity to system conditions [1]-[5]. The APFs are the power electronic converters with two or more passive elements, which provide harmonic and reactive power compensation at the PCC by using advanced algorithms. The APFs offer flexibility and, effective harmonic compensation and resonance elimination at the price of a higher cost and compromised reliability. Furthermore, at relatively high switching frequencies, the majority of power semiconductor switches are unable to carry high currents and block high voltages [6]-[9]. Traditional HAPFs consist of a single or multi-tuned PPF in series with the APF and can be readily employed in high-voltage networks. This construction leads to a noticeable decrease in the APF voltage rating, as the grid voltage fundamental component falls on the PPF capacitor. Therefore, the DC-link voltage of the converter is reduced along with its power and losses. However, because of the series connection, the converter semiconductor switches are subject to a high compensation current, which limits the use of these HAPFs in high-power applications [10]-[14]. The HAPF compensation current is even bigger than that of an APF alone. Also, if a fault occurs in the APF, the whole compensation current will be lost.

In [15]-[18], an improved structure of HAPF is introduced. This structure includes an APF in parallel with the single-tuned PPF inductor. This type of connection offers a reduced converter current and power and higher reliability than the traditional HAPFs at the price of the complexity of the control system and RCG. Although this configuration is presented for single-tuned PPFs, the exact modelling, design and control of the system and the effect of the model parameters variations on

Mohammad-Sadegh Karbasforooshan is with Ferdowsi University of Mashhad, Mashhad, Iran (e-mail: s.karbasforooshan@mail.um.ac.ir)
Mohammad Monfared is with Swansea University, SA1 8EN Swansea, UK, and with Ferdowsi University of Mashhad, Mashhad, Iran (e-mail: mohammad.monfared@swansea.ac.uk, m.monfared@um.ac.ir).

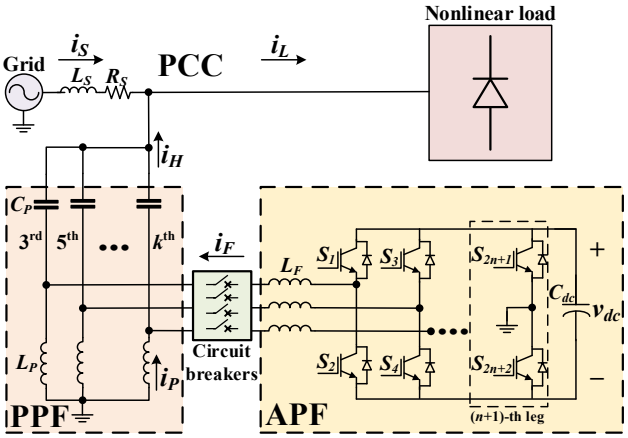

Fig. 1. Single-phase multi-tuned shunt HAPF.

the system stability and performance are not investigated in the previous works. While authors in [15] described the filtering characteristics and used a simple proportional controller, the system modelling, the parameters design and the control system design are not mentioned. In [16], the operation principle of the single-phase HAPF structure and a relatively complicated control system are presented, although, the grid current quality and the THD improvement are not impressive. In [17], the authors proposed modelling of the three-phase three-wire HAPF structure in αβ reference frame and a model-based controller design is described. However, the control structure of [17] is very sensitive to grid frequency changes. In [18], the authors proposed modelling and designing an adaptive self-tuned current controller for the single-phase single-tuned shunt HAPF. This control technique is relatively complex with a high computation burden. Also, the closed-loop stability of the control system against wide model parameter uncertainties is not investigated in [18]. In many industrial plants, there are multi-tuned PPFs which are tuned at 3rd, 5th, 7th, 9th … for single-phase systems (or three-phase four-wire systems) and 5th, 7th, 11th, 13th … for three-phase three-wire systems [2]-[4]. The APF of the structure of [15]-[18] can only be connected to one LC branch and the occurrence of the resonance between other branches and the grid remains unsolved. On the other hand, if each PPF inductor branch is connected to an APF, more than one APF is required and the cost increases. The single-phase shunt HAPF is intended for three-phase four-wire distribution networks to tackle the harmonics of a single or a group of domestic and commercial consumers.

Different control approaches are presented for the HAPF system in the literature. Each of these methods offers some of the desired goals of fast dynamic response, low steady-state tracking error, low computational burden, low sensitivity to model parameter variations, etc. Proportional [19], proportional-resonant [8], [14], fuzzy [20], repetitive [21], deadbeat [9], [11]-[12], model predictive [22], and nonlinear controllers [13], [23] are some of the common approaches, which can be categorized into model-based and non-model-based control techniques. The deadbeat control method is a model-based current control technique which is used in APF and HAPF control loops [9], [11]-[12]. This control technique offers simplicity, high control precision, low computational burden, and fast dynamic response. This method, however, is sensitive to changes in model parameters that can even lead to control system instability. Besides, the reference current tracking performance of the traditional deadbeat controller is adversely affected by sampling errors [11]-[12]. However, this problem is solved by introducing the predictive deadbeat technique [9]. This paper develops a predictive deadbeat current controller that is adaptive and has low sensitivity to model parameter mismatches as the control gains are corrected automatically and online.

In this paper, first, the circuit configuration of a generic single-phase multi-tuned shunt HAPF is presented. This topology reduces the converter currents and eliminates the possibility of resonance between the multi-tuned PPF and the grid. This is followed by an exact modelling and controller design. The proposed structure can be employed with single-phase and three-phase four-wire loads. Moreover, its generality allows it to be implemented in any industry that already has multi-tuned PPFs installed. The advantages of the developed compensator are generality, further reducing the converter currents, reducing the cost, and increasing reliability. The original contributions of this paper can be listed as:

- proposing a generic single-phase multi-tuned shunt HAPF;
- exact modelling of the proposed high-order system;
- designing an adaptive predictive deadbeat current controller for the HAPF system;
- evaluating the stability of the closed-loop digital control system against model parameters variations;
- evaluating the effectiveness of the proposed system through extensive simulations and experiments;
- demonstrating the superiority of the suggested structure over some other conventional solutions through comparisons.

The paper is organized as follows: Section II describes the proposed system configuration followed by section III on modelling the high-order system. In section IV, the parameter design is explained and section V presents the RCG and design of the proposed controller for the HAPF system. Simulation and experimental verifications are reported in section VI. Finally, section VII concludes the paper.

II. System Configuration

The proposed system configuration is shown in Fig. 1. In this figure, the proposed HAPF is a combination of a multi-tuned PPF and an APF, which is in parallel with the PPF inductors. The conventional multi-tuned PPF has its branches tuned at the 3rd, 5th, …, kth harmonic orders and the APF consists of an (n+1)-leg converter with the output filters. Each leg of the APF converter is in parallel with each inductor of the multi-tuned PPF and (n+1)-th leg is connected to the neutral. A circuit breaker (CB) connects each APF leg to the PPF inductor, offering more flexibility and reliability to the system. The flowchart of the activation algorithm for the APF branches can be seen in Fig. 2. As can be observed, first the number of PPF branches and the desired compensation level ($0 \le D_m \le 1$) are fed to the algorithm. This variable (D_m) is defined as a ratio between the harmonics RMS current and total RMS current ($m \ge 3$).

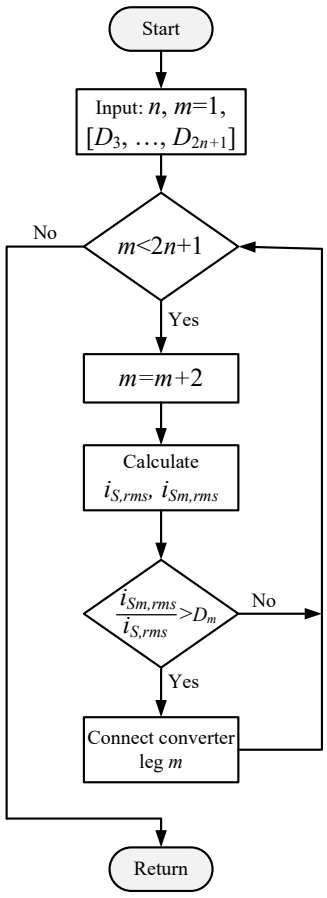

Fig. 2. Proposed activation algorithm for the performance of the APF.

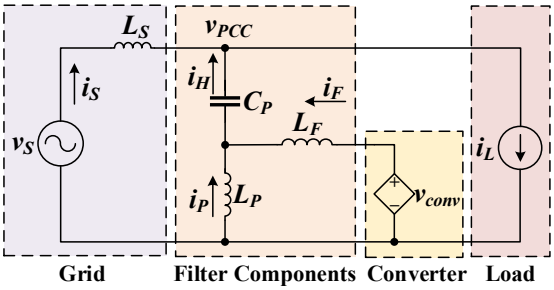

Fig. 3. Structure of a single-phase single-tuned shunt HAPF.

Therefore, the lower the D_m, the lower the total harmonic distortion. The proper value for D_m should be selected according to system configuration and the power capacity. It decides on the required converter legs that must be activated till the required compensation is reached. If more than one leg is connected to the PPF, the APF injected current is divided among n-legs reducing the current through each converter leg. Each converter leg is responsible for the compensation of a group of harmonic components. For example, in single-phase systems, if n=1, a full-bridge converter should compensate the whole harmonic components; if n=2 and if needed, the first leg, which is connected to the third harmonic branch of the PPF dominantly compensates for the 3k harmonic components and the second leg, which is connected to the fifth harmonic branch can compensate for the 6k±1 harmonic components and so on. It should be noted that the fundamental structure is a single-phase single-tuned shunt HAPF (n=1). This fundamental structure is responsible for the whole harmonic compensation. If needed and the compensation capacity is not sufficient, according to the mentioned decision algorithm, the converter legs can be activated.

III. High-Order System Modelling

A. Single-Phase Single-Tuned Shunt HAPF Modelling

In this section, first, the single-phase single-tuned shunt HAPF model is developed and then generalized to the multi-tuned shunt HAPF. A single-phase single-tuned shunt HAPF is displayed in Fig. 3. In this figure, the grid is modelled as a sinusoidal voltage source (v_S) with an inductive series impedance and the load as an independent current source (i_L). Also, the filter components are PPF capacitor, PPF inductor and converter output inductor and the converter is assumed as a dependent voltage source (v_{conv}). The KVL and KCL equations for Fig. 2 in the Laplace form yield

$$\begin{bmatrix} i_F(s) \\ i_H(s) \\ i_S(s) \end{bmatrix} = \underbrace{\begin{bmatrix} (L_F+L_P)s & -L_P s & 0 \\ L_P s & -\left(L_P s+\dfrac{1}{C_P s}\right) & 0 \\ 0 & 1 & 1 \end{bmatrix}^{-1}}_{M} \begin{bmatrix} v_{conv}(s) \\ v_{PCC}(s) \\ i_L(s) \end{bmatrix}. \quad (1)$$

Reactive elements have an ESR, which contributes to damping in filter characteristics and reduces the resonance peak. The transfer functions of the converter output voltage to the APF and the HAPF injected currents are calculated as

$$Y_F(s)=\frac{i_F(s)}{v_{conv}(s)}=\frac{L_P C_P s^2+1}{L_F L_P C_P s^3+(L_F+L_P)s} \quad (2)$$

$$Y_H(s)=\frac{i_H(s)}{v_{conv}(s)}=\frac{L_P C_P s^2}{L_F L_P C_P s^3+(L_F+L_P)s}. \quad (3)$$

To transform $Y_F(s)$ to digital domain, the Tustin discretization method is employed. This approach has the advantages of accurate approximation of the continuous transfer functions and that the left half s-plane is transformed into the unit circle. So, the stable continuous-time systems are transformed into stable discrete-time systems. Therefore, $Y_F(s)$ in discrete-time form is

$$Y_F(z)=\frac{i_F(z)}{v_{conv}(z)}=\frac{b_1 z^3+b_2 z^2+b_2 z+b_1}{z^3+a_1 z^2-a_1 z-1}$$

$$\begin{bmatrix} b_1 \\ b_2 \\ a_1 \end{bmatrix} = \frac{1}{T_S^2(L_F+L_P)+4L_F L_P C_P} \begin{bmatrix} 0.5T_S^3+2L_P C_P T_S \\ 1.5T_S^3-2L_P C_P T_S \\ T_S^2(L_F+L_P)-12L_F L_P C_P \end{bmatrix} \quad (4)$$

As can be seen, $Y_F(z)$ has three independent parameters in its numerator and denominator (b_1, b_2 and a_1). The HAPF model elements can be easily found from these parameters as

$$\begin{cases} L_F=\dfrac{T_S(1-a_1)}{6b_1-2b_2}, \quad C_P=\dfrac{T_S(3b_1-b_2)^2}{8(2b_1-b_2+a_1 b_1)} \\ L_P=\dfrac{2T_S(2b_1-b_2+a_1 b_1)}{(b_1+b_2)\times(3b_1-b_2)} \end{cases}. \quad (5)$$

B. Single-Phase Multi-Tuned Shunt HAPF Modelling

Following the same procedure for the single-phase single-tuned shunt HAPF, the KVL and KCL equations for the multi-tuned shunt HAPF are obtained as (6).

$$\begin{bmatrix} i_{F,3}(s) \\ i_{H,3}(s) \\ \vdots \\ i_{F,k}(s) \\ i_{H,k}(s) \\ i_S(s) \end{bmatrix} = \underbrace{\begin{bmatrix} [Z_3]_{2\times2} & \cdots & [0]_{2\times2} & [B]_{2\times1} \\ \vdots & \vdots & \vdots & \vdots \\ [0]_{2\times2} & \cdots & [Z_k]_{2\times2} & [B]_{2\times1} \\ [C]_{1\times2} & \cdots & [C]_{1\times2} & 1 \end{bmatrix}^{-1}}_{M} \begin{bmatrix} v_{conv,3}(s) \\ v_{PCC}(s) \\ \vdots \\ v_{conv,k}(s) \\ v_{PCC}(s) \\ i_L(s) \end{bmatrix}. \quad (6)$$

$$B = \begin{bmatrix} 0 & 0 \end{bmatrix}^T \qquad C = \begin{bmatrix} 0 & 1 \end{bmatrix}$$

As can be seen, M is a $(2n+1)\times(2n+1)$ sparse matrix. The matrix Z_k, given in (7), is a 2×2 matrix.

$$Z_k = \begin{bmatrix} (L_{F,k} + L_{P,k})s & -L_{P,k}s \\ L_{P,k}s & -\left(L_{P,k}s + \dfrac{1}{C_{P,k}s}\right) \end{bmatrix}. \quad (7)$$

Therefore, Z_k is located in the main diagonal of M, except for the last row, and the voltages and currents of each LC branch of PPF, which is connected to the output filter of one leg of the converter, are independent of other branches. The latest row of M implies that the sum of HAPF currents and the grid current equals the load current. From (6), the transfer function between different sections of multi-tuned HAPF can be obtained.

IV. High-Order System Parameter Design

A. Parameter Design of Single-Phase Single-Tuned Shunt HAPF

To design the parameters of the system depicted in Fig. 2, first PPF parameters should be designed. These parameters determine the reactive power capacity of PPF and the tuned frequency of the filter. The reactive power capacity of PPF is based on the type of nonlinear load. Based on the reactive power requirements and the harmonic order of the filter, its capacitance is calculated as

$$C_P = \left(1 - \frac{1}{h^2}\right)\frac{Q_L}{2\pi f_1 V_S^2} \quad (8)$$

where h, Q_L, f_1 and V_S are the tuned harmonic order, reactive power capacity, fundamental frequency and the RMS grid voltage, respectively. Therefore, the inductor value can be easily obtained from the tuned harmonic order of the branch as

$$L_P = \frac{1}{\left(h \cdot 2\pi f_1\right)^2 \cdot C_P}. \quad (9)$$

To design the APF output inductor, the converter current ripple should be considered. Therefore, in this paper, a certain percentage of the nominal peak current, x_L, is used to limit the converter current ripple. This relationship is stated in (10), where x_L=0.15-0.4, and V_{dc}, T_S, $I_{P,rated}$ are the DC-link voltage of the converter, sampling time, and converter nominal peak current, respectively.

$$\left(\Delta i_{I,\max} = \frac{V_{dc}T_S}{8L_F}\right) \le x_L I_{P,rated}. \quad (10)$$

B. Parameter Design of Single-Phase Multi-Tuned Shunt HAPF

Similar to the above procedure, other PPF and APF parameters can be easily calculated according to (8)-(10). It should be noticed that the PPF inductor and capacitor are different for each branch. The APF output inductance of each branch depends on V_{dc}, T_S, x_L, and $I_{P,rated}$. The parameters V_{dc} and T_S are the same for all branches, but x_L and $I_{P,rated}$ are different. For simplicity, the multiplication of these two parameters is considered the same. So, the APF output inductor is assumed the same for all branches, as given by (10).

V. RCG and Control System Design

A. RCG

SOGI is a well-known technique for many applications such as grid synchronization and harmonic extraction. Several variations of this structure have been developed, including the multi-SOGI [24]. Each of the SOGI units in parallel is tuned at the specific harmonic frequency to extract this harmonic component in the output of the multi-SOGI. In this paper, odd harmonic components of the load current below the 25th order are extracted by the multi-SOGI and the PPF inductor current is subtracted from the sum of these harmonic currents to obtain the APF reference current. The current control loop uses the APF injected current, i_F.

B. Adaptive Predictive Deadbeat Current Control System Design

The HAPF control system is based on an adaptive digital predictive deadbeat controller mainly inspired by a procedure proposed in [9]. A system identification method is then also proposed to estimate the model parameters. To determine the switching pattern, the control signal is calculated for all legs of the converter except for the $(n+1)$-th. The latest leg control signal is obtained as the sum of all other control signals with an opposite sign. The KVL for each leg of the converter is

$$v_{conv} + v_{C_P} - v_{PCC} = L_F \frac{di_F}{dt} \quad (11)$$

where v_{Cp} is the voltage across the PPF capacitor.

By ignoring the slight changes in the grid and PPF capacitor voltages during the short sampling period, (11) can be approximated as (12) in the discrete-time domain.

$$\begin{cases} i_F\left[(k+d)T_s\right] - i_F\left[kT_s\right] = dT_s \dfrac{v_{C_P} + v_{dc} - v_{PCC}}{L_F} \\ i_F\left[(k+1)T_s\right] - i_F\left[(k+d)T_s\right] = (1-d)T_s \dfrac{v_{C_P} - v_{dc} - v_{PCC}}{L_F} \end{cases}. \quad (12)$$

With a double update PWM modulator (sampling frequency is twice the switching frequency), the duty cycle of the PWM signal in the k-th instance is calculated as

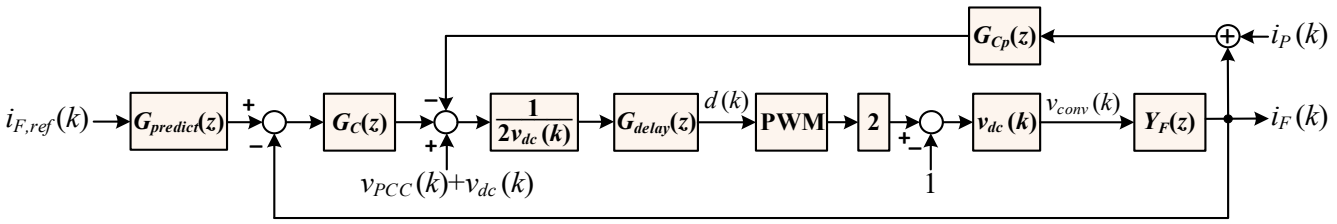

Fig. 4. Block diagram of the current control system.

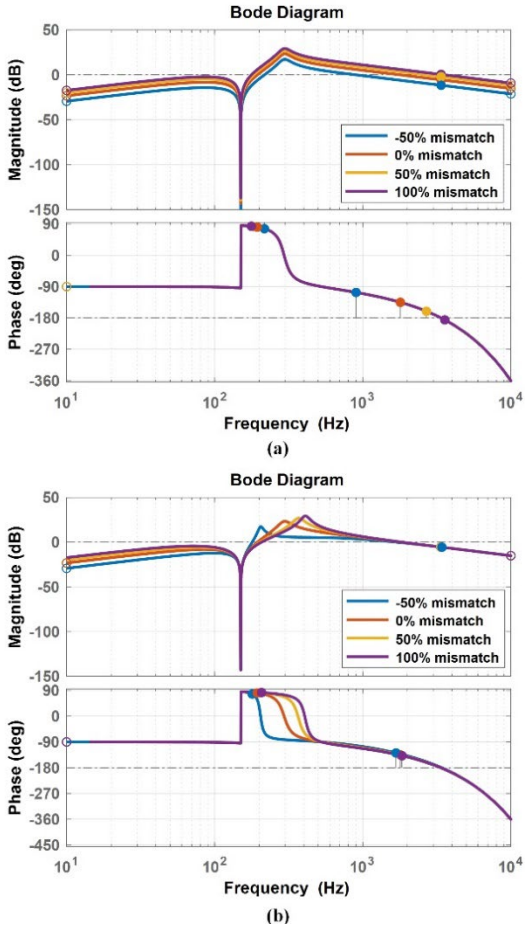

Fig. 5. Bode diagram of the open-loop current control system considering mismatches in (a) L_F, (b) C_P.

$$d[k]=\frac{L_F\left(i_F[(k+1)T_s]-i_F[kT_s]\right)}{2v_{dc}[kT_s]T_s}+\frac{v_{dc}[kT_s]+v_{PCC}[kT_s]-v_{C_P}[kT_s]}{2v_{dc}[kT_s]} \quad (13)$$

which shows that the duty cycle includes feedback of the current error plus feedforwards of the grid and PPF capacitor voltages. The PPF capacitor voltage is obtained from its current using the Backward Euler method, as

$$v_{C_P}[kT_s]=v_{C_P}[(k-1)T_s]-\frac{T_s}{C_P}\left(i_F[kT_s]+i_P[kT_s]\right). \quad (14)$$

The control objective is to make the injected current by the APF track its reference closely. So, it is replaced in (13) by the reference current at the next sampling instance. In this paper, the next sample reference current is estimated from the two previous samples as already reported in [9].

The current control loop scheme is depicted in Fig. 4, where $G_{predict}(z)=(1+z^{-1}-z^{-2})$ is the APF reference current predictor, $G_C(z)=L_F/T_s$ is the control system gain, $G_{Cp}(z)=(T_s/C_p)\times z/(z-1)$ is the estimator of the PPF capacitor voltage, $G_{delay}(z)=z^{-Td/Ts}$ is the digital controller delay function (T_d is assumed $1.5T_s$ for a double-updated PWM modulator) and $Y_F(z)$ is the plant discretized model. Based on Fig. 4, the transfer function of the closed-loop current control system is obtained as

$$H_{closed}(z)=\frac{i_F(k)}{i_{F,ref}(k+1)}=\frac{G_C(z)G_{delay}(z)Y_F(z)}{1+G_C(z)G_{delay}(z)Y_F(z)}. \quad (15)$$

Figures 5(a) and (b) show the open-loop Bode diagram of the APF current control system, considering mismatches in the L_F and C_P values. When L_F uncertainty varies from -50% to +100%, the magnitude characteristic slightly rises. Therefore, the system phase margin decreases as L_F is overestimated in the algorithm. When L_F uncertainty equals +100%, the phase characteristic crosses -180º at 0 dB and the control system is unstable. To demonstrate the stability of the control system against PPF capacitor mismatches, its uncertainty changed from -50% to +100%. Figure 5(b) shows the Bode diagram of the open-loop current control system. According to Fig. 5(b), the gain and phase margins of the system do not change. However, the frequency of the resonance slightly increases. The control system remains stable under a large mismatch of the PPF capacitor.

C. System Identification

The proposed deadbeat control approach uses APF output inductor and PPF capacitor values, which may not be always known or can vary by several factors such as temperature, ageing, tolerances, deterioration, etc. The effect of possible mismatches on the system stability was studied in the previous subsection. Besides that, any deviation from the nominal values, which are considered in the control law inversely affects the system's performance. In this paper, the correct instantaneous values of the inductor and the capacitor are estimated online and used in the control law. To do this, the difference equation of (4) is rewritten as

$$\underbrace{\left(i_F(k)-i_F(k-3)\right)}_{\tilde{i}_F(k)}=a_1\left(-i_F(k-1)+i_F(k-2)\right)+b_1\left(v_{conv}(k)+v_{conv}(k-3)\right)+b_2\left(v_{conv}(k-1)+v_{conv}(k-2)\right) \quad (16)$$

So, the identification regression vector is

$$\varphi(k)=\begin{bmatrix}-i_F(k-1)+i_F(k-2)\\ v_{conv}(k)+v_{conv}(k-3)\\ v_{conv}(k-1)+v_{conv}(k-2)\end{bmatrix} \quad (17)$$

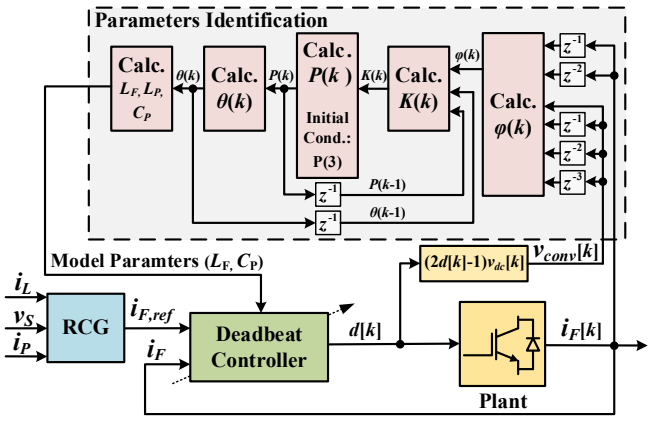

Fig. 6. Overall control system structure.

TABLE I
Plant Parameters

Parameter	Symbol	Value
Grid voltage (RMS)	V_S	220 Vrms
Grid frequency	f	50 Hz
APF nominal apparent power	S_{rated}	1 kVA
DC-link voltage	V_{DC}	150 V
3rd branch PPF capacitor	$C_{P,3}$	100 µF
3rd branch PPF inductor	$L_{P,3}$	11.25 mH
Converter output inductor	L_F	1 mH
Switching/sampling frequency	f_{sw}/f_s	10/20 kHz

and the identification parameters are

$$\theta^T(k)=\begin{bmatrix} a_1 & b_1 & b_2 \end{bmatrix}. \tag{18}$$

The RLS estimation technique for the current system identification can be then formulated as

$$\begin{cases} \begin{bmatrix} \hat{a}_1(k) \\ \hat{b}_1(k) \\ \hat{b}_2(k) \end{bmatrix} = \begin{bmatrix} \hat{a}_1(k-1) \\ \hat{b}_1(k-1) \\ \hat{b}_2(k-1) \end{bmatrix} \\ +K(k)\times \begin{pmatrix} \tilde{i}_F(k)-\hat{a}_1(k-1)\times(-i_F(k-1)+i_F(k-2)) \\ -\hat{b}_1(k-1)\times(v_{conv}(k)+v_{conv}(k-3)) \\ -\hat{b}_2(k-1)\times(v_{conv}(k-1)+v_{conv}(k-2)) \end{pmatrix} \\ K(k)=\dfrac{P(k-1)\varphi(k)}{\lambda+\varphi^T(k)P(k-1)\varphi(k)} \\ P(k)=\left(I_3-K(k)\begin{bmatrix} -i_F(k-1)+i_F(k-2) \\ v_{conv}(k)+v_{conv}(k-3) \\ v_{conv}(k-1)+v_{conv}(k-2) \end{bmatrix}^T\right)\dfrac{P(k-1)}{\lambda} \end{cases} \tag{19}$$

where λ is the forgetting factor of the estimation technique used to increase the weight of recent data compared to older ones [25]. After identifying the system and determining a_1, b_1 and b_2, the inductor and the capacitor can be easily calculated from (5). Figure 6 shows the overall structure of the proposed control system. As can be seen, the measured APF injected current and the calculated converter voltage at current and previous samples

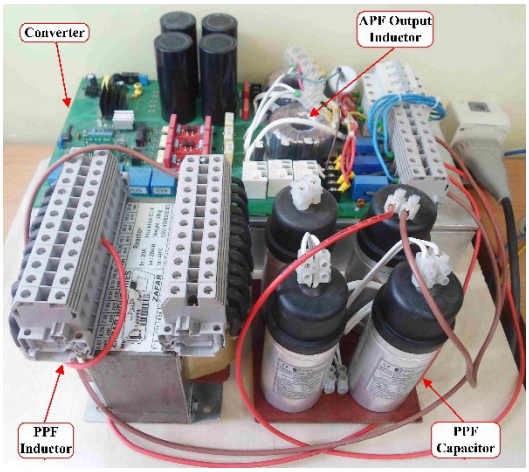

Fig. 7. Experimental setup.

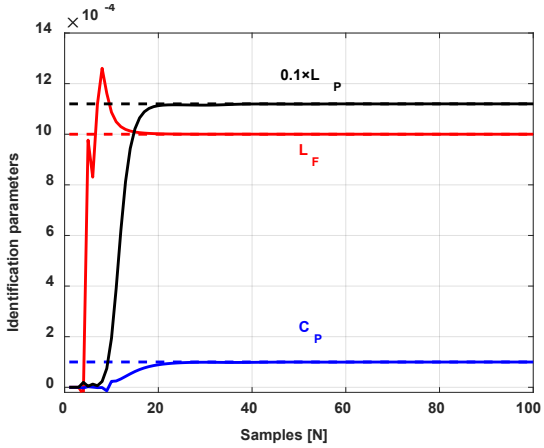

Fig. 8. HAPF identified parameters (L_F, L_P and C_P).

are fed to the identification block and this block outputs the model parameters (L_F, L_P and C_P). Accordingly, the proposed control system continuously corrects the deadbeat controller gain. Consequently, variations in model parameters do not have a significant impact on controller performance.

VI. Simulation and Experimental Results

Simulation and experimental results are provided in this section to confirm the proper performance of the proposed controller for the suggested HAPF. MATLAB/Simulink software is used for simulations. A laboratory single-phase single-tuned shunt HAPF is also built, which is shown in Fig. 7. The designed system parameters are summarized in Table I. A 4.5 kVA single-phase full-wave diode rectifier is connected to the PCC for both laboratory experiments and simulations. The control scheme is executed on a STM32F407VGT6 32-bit digital microcontroller from STMicroelectronics. The grid voltage THD is 4.5%. The simulation and experimental results for a single-tuned (the 3rd harmonic) shunt HAPF are reported, first. The identified parameters are shown in Fig. 8 (L_F and C_P). As can be seen, the HAPF parameters are estimated precisely in less than 20 samples. Figure 9 shows the steady-state results. Figure 9(a) shows the experimental steady-state grid, load, PPF inductor and APF injected currents when only the PPF is worked. The load and the grid current harmonic spectrums are shown in Figs. 10 (a) and (b) under this condition. The

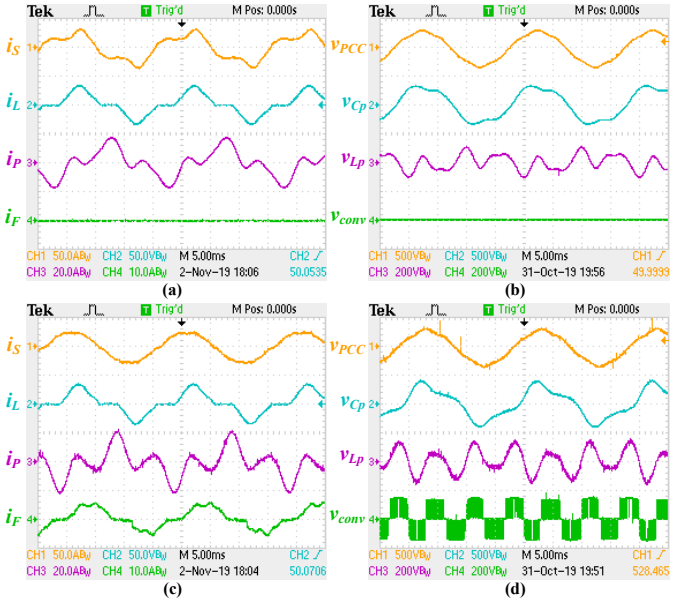

Fig. 9. Steady-state experimental results: (a) grid current, load current, PPF inductor current and APF injected current, and (b) grid voltage, PPF capacitor voltage, PPF inductor voltage and converter output voltage when only PPF is worked, (c) grid current, load current, PPF inductor current and APF injected current, and (d) grid voltage, PPF capacitor voltage, PPF inductor voltage and converter output voltage when HAPF is also activated.

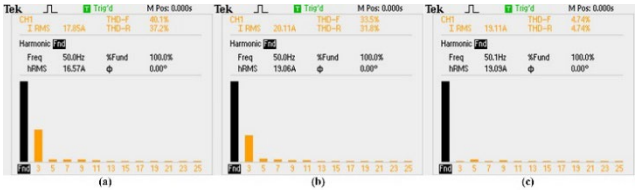

Fig. 10. Experimental harmonic spectrums of (a) load current, (b) grid current when only PPF is connected to PCC, (c) grid current when HAPF is also activated.

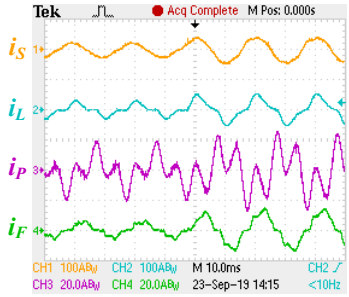

Fig. 11. Transient experimental results in response to load sudden change: grid current, load current, PPF inductor current and APF injected current.

experimental load current THD is about 40% and the grid current THD decreases to 33.5% with the operation of the PPF. So, just a small improvement in the grid's current quality is achieved. Figure 9(b) illustrates the steady-state grid, PPF capacitor, PPF inductor and converter output voltages, respectively, under this condition. As can be observed, the converter output voltage and the APF injected current are both zero. The experimental results with the APF in action are also depicted in Figs. 9(c) and (d). With the APF connected to the system, the grid current THD decreases to 4.74% and its quality is much better than before. The harmonic spectrum of the grid current is displayed in Fig. 10 (c), where the major harmonic components (3rd, 5th, 7th and 9th) have been successfully damped. These figures imply that with a moderate APF current,

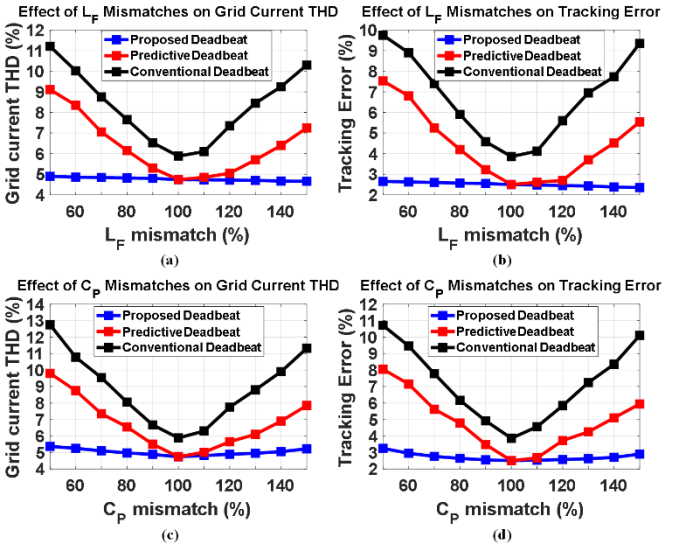

Fig. 12. Effect of model parameters mismatches on the performance of three deadbeat control system: (a) effect of L_F mismatches on grid current THD, (b) effect of L_F mismatches on current tracking error, (c) effect of C_P mismatches on grid current THD, (d) effect of C_P mismatches on current tracking error.

perfect harmonic compensation is achieved. Also, the operation of the APF within the proposed HAPF structure improves the performance of the PPF itself, as it more effectively and selectively bypasses only the third harmonic component of the load current (which is already tuned at this harmonic order), as depicted in Fig. 9(c). The experimental results for a single-tuned shunt HAPF in Figs. 9 and 10 describe the successfulness and appropriate performance of the proposed system. To evaluate the transient treatment of the compensation system, the response to load sudden change is reported in Fig. 11. It can be seen that, after a large load change (more than 50% increase), the controller performs very fast, and the APF injected current and the grid current reach steady-state in less than a quarter cycle. Also, it can be seen that following a load current change, the APF reference current changes fast and the APF injected current tracks the reference fast and with minimum error. Also, the grid's current THD remains under 5%. To compare the proposed current control technique with the conventional ones in presence of model parameters uncertainties, conventional deadbeat [11]-[12] and predictive deadbeat [9] are also implemented alongside the proposed adaptive predictive deadbeat controller. The effect of the converter output inductor uncertainties and PPF capacitor uncertainties on the grid current THD and the APF current tracking error is reviewed and the results are drawn in Figs. 12 (a), (b), (c) and (d). As can be observed, the wide range of mismatches of L_F and C_P has a destructive effect on both the conventional and the predictive deadbeat controllers, while it cannot affect the proposed adaptive predictive deadbeat controller. The suggested controller adaptively changes the control gain according to the estimated HAPF parameters, while for the two other controllers, the control gain remains constant.

Finally, a different type of nonlinear load that has high magnitude 5th and 7th order harmonic currents is connected to PCC. Also, a double-tuned (at the 3rd and 5th harmonics) shunt PPF is constructed and a small D_5 is used for the proposed algorithm. So, a three-leg converter is connected to the multi-

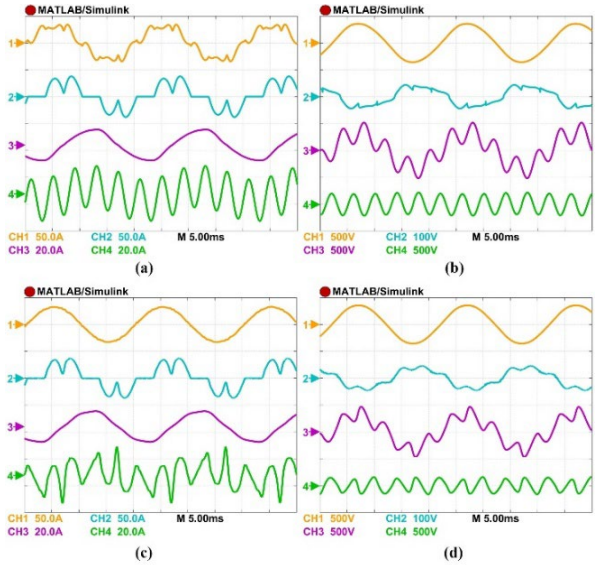

Fig. 13. Steady-state simulation results: (a) grid current, load current, 3rd PPF capacitor current and 5th PPF capacitor current, and (b) 3rd PPF capacitor voltage, 3rd inductor voltage, 5th PPF capacitor voltage and 5th inductor voltage when only PPF is worked, (c) grid current, load current, 3rd PPF capacitor current and 5th PPF capacitor current, and (d) 3rd PPF capacitor voltage, 3rd inductor voltage, 5th PPF capacitor voltage and 5th inductor voltage when HAPF is also activated.

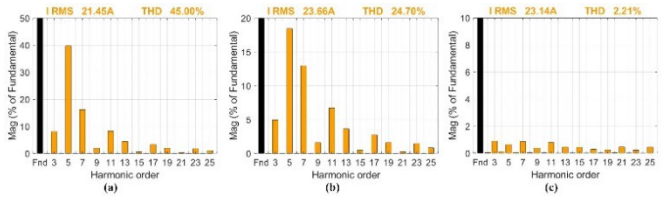

Fig. 14. Simulation harmonic spectrums of (a) load current, (b) grid current when only PPF is connected to PCC, (c) grid current when HAPF is also activated.

TABLE II
Comparison among various harmonic compensation solutions

	Grid current THD	PPF RMS current	APF RMS current	Converter DC-link voltage	Conv erter power	Active elements
PPF (3rd tuned)	33.5%	9.15 A_{rms}	0	0	0	---
APF [8]-[10]	2.5%	0	6.5 A_{rms}	400 V	1800 VA	4 switch (400V/13A)
Conventional HAPF [14], [15]	3.5%	9.75 A_{rms}	9.75 A_{rms}	150 V	780 VA	4 switch (400V/13A)
Proposed HAPF (Fig. 2)	4%	9.15 A_{rms}	3.10 A_{rms}	150 V	310 VA	4 switch (400V/13A)

tuned PPF to construct a multi-tuned HAPF. The simulation results are shown in Fig. 13. Figure 13 (a) depicts the steady-state grid, load, 3rd PPF capacitor and 5th PPF capacitor currents, respectively, when only the 3rd and 5th PPFs are connected to the PCC. Figures 14 (a) and (b) demonstrate the harmonic spectrums of the load and grid currents under this condition. From the figures, the load current THD is 45% (with the major harmonic components of the fifth and seventh) and the grid current THD decreases to 24.7% with the PPFs. Figures 13 (c) and (d) show the waveforms when the APF is also working. When the APF connects to the system, the grid current THD reduces to 2.21% (as shown in Fig. 14 (c)), and all harmonic components are limited well below 1% of the fundamental component. Now, each converter leg injects its relevant harmonic current (3k harmonic components by the first leg, which is connected to the 3rd PPF and 6k±1 harmonic components by the second leg, which is connected to the 5th PPF) and with the APF, both PPFs draw only the tuned harmonic currents. These results confirm the proper performance of the double-tuned HAPF.

Table II compares different harmonic compensation techniques (single-phase structures) for the single-phase loads. As can be observed, except for the PPF, which has no active element, the other three compensators offer good harmonic compensation performance as the grid current THD is within the standard limit. Among the three solutions, the proposed system has the lowest APF injected current and power and the lowest overall rating, which results in lower converter loss and cost.

VII. Conclusion

This paper proposed an adaptive predictive deadbeat control method for the single-phase shunt HAPF topology. The advantages of the proposed power structure are generality, simplicity, and minimum converter currents and it can be used with the already installed multi-tuned PPFs. The presented high-order electric system is first modelled; then a straightforward step-by-step design approach for the single-tuned and multi-tuned HAPF is proposed. The RCG and an adaptive predictive deadbeat control system design are illustrated and the closed-loop current control system stability against the model parameter mismatches is investigated. To validate the theoretical results, experimental results for a single-phase single-tuned shunt HAPF and simulation results for a single-phase double-tuned shunt HAPF are reported. These results show that the designed high-order structure compensates for the harmonic currents effectively and enhances the PPF filtering characteristics with relatively low APF current requirements. In addition, performance comparisons with two conventional solutions are provided to demonstrate the superiority of the suggested filtering system.

VIII. References

[1] J. C. Das, "Passive filters—potentialities and limitations," *IEEE Trans. Ind. Appl.*, vol. 40, no. 1, pp. 232–241, Jan. 2004.

[2] A. B. Nassif, Wilsun Xu, and W. Freitas, "An Investigation on the selection of filter topologies for passive filter applications," *IEEE Trans. Power Deliv.*, vol. 24, no. 3, pp. 1710–1718, Jul. 2009.

[3] P. Salmeron and S. P. Litran, "Improvement of the electric power quality using series active and shunt passive filters," *IEEE Trans. Power Deliv.*, vol. 25, no. 2, pp. 1058–1067, Apr. 2010.

[4] H. Hu, Z. He, and S. Gao, "Passive filter design for china high-speed railway with considering harmonic resonance and characteristic harmonics," *IEEE Trans. Power Deliv.*, vol. 30, no. 1, pp. 505–514, Feb. 2015.

[5] M. Babaei and M. Monfared, "High step-down bridgeless sepic/cuk PFC rectifiers with improved efficiency and reduced current stress," *IEEE Trans. Ind. Electron.*, vol. 69, no. 10, pp. 9984–9991, Oct. 2022.

[6] M. Badoni, A. Singh, and B. Singh, "Variable forgetting factor recursive least square control algorithm for DSTATCOM," *IEEE Trans. Power Deliv.*, vol. 30, no. 5, pp. 2353–2361, Oct. 2015.

[7] M.-S. Karbasforooshan and M. Monfared, "An adaptive recursive discrete Fourier transform technique for the reference current generation of single-

phase shunt active power filters," in *7th Power Electron. Drive Syst. Technol. Conf. (PEDSTC)*, pp. 253-259, Feb. 2016.
[8] M.-S. Karbasforooshan and M. Monfared, "Multi-resonant indirect digital current control technique for single-phase shunt active power filters," *Electr. Power Components Syst.*, vol. 47, no. 13, pp. 1196–1202, Nov. 2019.
[9] M.-S. Karbasforooshan and M. Monfared, "An improved reference current generation and digital deadbeat controller for single-phase shunt active power filters," *IEEE Trans. Power Deliv.*, vol. 35, no. 6, pp. 2663–2671, Dec. 2020.
[10] H. M. A. Antunes, I. A. Pires, and S. M. Silva, "Evaluation of series and parallel hybrid filters applied to hot strip mills with cycloconverters," *IEEE Trans. Ind. Appl.*, vol. 55, no. 6, pp. 6643–6651, Nov. 2019.
[11] Yang Han, Lin Xu, M. M. Khan, Chen Chen, Gang Yao, and Li-Dan Zhou, "Robust deadbeat control scheme for a hybrid APF with resetting filter and ADALINE-based harmonic estimation algorithm," *IEEE Trans. Ind. Electron.*, vol. 58, no. 9, pp. 3893–3904, Sep. 2011.
[12] W.-K. Sou, W.-H. Choi, C.-W. Chao, C.-S. Lam, C. Gong, C.-K. Wong, and M.-C. Wong, "A deadbeat current controller of LC-hybrid active power filter for power quality improvement," *IEEE J. Emerg. Sel. Top. Power Electron.*, vol. 8, no. 4, pp. 3891–3905, Dec. 2020.
[13] C. Gong, W.-K. Sou, and C.-S. Lam, "Second-order sliding mode current controller for LC-coupling hybrid active power filter," *IEEE Trans. Ind. Electron.*, vol. 68, no. 3, pp. 1883–1894, Mar. 2021.
[14] C. Gong, W.-K. Sou, and C.-S. Lam, "Design and analysis of vector proportional–integral current controller for LC- coupling hybrid active power filter with minimum DC-link voltage," *IEEE Trans. Power Electron.*, vol. 36, no. 8, pp. 9041–9056, Aug. 2021.
[15] J.-C. Wu, H.-L. Jou, H.-H. Hsaio, and S.-T. Xiao, "A new hybrid power conditioner for suppressing harmonics and neutral-line current in three-phase four-wire distribution power systems," *IEEE Trans. Power Deliv.*, vol. 29, no. 4, pp. 1525–1532, Aug. 2014.
[16] Y. Deng, X. Tong, and H. Jia, "A bidirectional control principle of active tuned hybrid power filter based on the active reactor using active techniques," *IEEE Trans. Ind. Informatics*, vol. 11, no. 1, pp. 141–154, Feb. 2015.
[17] A. A. Valdez-Fernandez, G. Escobar, P. R. Martinez-Rodriguez, J. M. Sosa, D. U. Campos-Delgado, and M. J. Lopez-Sanchez, "Modelling and control of a hybrid power filter to compensate harmonic distortion under unbalanced operation," *IET Power Electron.*, vol. 10, no. 7, pp. 782–791, Jun. 2017.
[18] M.-S. Karbasforooshan and M. Monfared, "Adaptive self-tuned current controller design for an LCL-filtered LC-tuned single-phase shunt hybrid active power filter," *IEEE Trans. Power Deliv.*, vol. 37, no. 4, pp. 2747–2756, Aug. 2022.
[19] T.-L. Lee, Y.-C. Wang, J.-C. Li, and J. M. Guerrero, "Hybrid active filter with variable conductance for harmonic resonance suppression in industrial power systems," *IEEE Trans. Ind. Electron.*, vol. 62, no. 2, pp. 746–756, Feb. 2015.
[20] P. Dey and S. Mekhilef, "Shunt hybrid active power filter under nonideal voltage based on fuzzy logic controller," *Int. J. Electron.*, vol. 103, no. 9, pp. 1–13, Feb. 2016.
[21] Lei Hong, Ye Tian, Jing Zhang, Dujiang Li, Dehong Xu, and Guozhu Chen, "High precision compensation for high power Hybrid Active Power Filter based on repetitive control algorithm," in *2011 IEEE International Symposium on Industrial Electronics*, 2011, pp. 295–300.
[22] S. C. Ferreira, R. B. Gonzatti, R. R. Pereira, C. H. da Silva, L. E. B. da Silva, and G. Lambert-Torres, "Finite control set model predictive control for dynamic reactive power compensation with hybrid active power filters," *IEEE Trans. Ind. Electron.*, vol. 65, no. 3, pp. 2608–2617, Mar. 2018.
[23] A. Hamadi, S. Rahmani, and K. Al-Haddad, "Digital control of a shunt hybrid power filter adopting a nonlinear control approach," *IEEE Trans. Ind. Informatics*, vol. 9, no. 4, pp. 2092–2104, Nov. 2013.
[24] P. Rodríguez, A. Luna, R. S. Muñoz-Aguilar, I. Etxeberria-Otadui, R. Teodorescu, and F. Blaabjerg, "A stationary reference frame grid synchronization system for three-phase grid-connected power converters under adverse grid conditions," *IEEE Trans. Power Electron.*, vol. 27, no. 1, pp. 99–112, 2012.
[25] K. J. Åström, and B. Wittenmark, *Adaptive Control*, Second Edition, Mineola, N.Y., USA: Dover Publications Inc., 2008.

Mohammad-Sadegh Karbasforooshan received the B.Sc., M.Sc. and Ph.D. degrees (all three with honors) in electrical engineering from Ferdowsi University of Mashhad, Mashhad, Iran, in 2013, 2015 and 2022, respectively. He is currently a Postdoctoral Researcher with the Power Electronics Laboratory, Faculty of Engineering, Ferdowsi University of Mashhad, Mashhad, Iran.

His research interests include control of standalone and grid-connected inverters, active and hybrid power filters, and power quality.

Mohammad Monfared (S'07, M'10, SM'15) received the B.Sc. degree in electrical engineering from Ferdowsi University of Mashhad, Iran, in 2004, and the M.Sc. and Ph.D. degrees (Hons.) in electrical engineering from Amirkabir University of Technology, Tehran, Iran, in 2006 and 2010, respectively. In 2022, he joined the Faculty of Science and Engineering, Swansea University, U.K. His current research interests include power electronics, renewable energy systems, and energy management. He is an Associate Editor of IEEE Transactions on Industrial Electronics..